Rolling optimization based on holism for the operation strategy of solar tower power plant

Chen Wang [a], Su Guo [a,*], Huanjin Pei [a], Yi He [a], Deyou Liu [a], Mengying Li [b]

[a] College of Energy and Electrical Engineering, Hohai University, Nanjing 211100, China
[b] Department of Mechanical Engineering, The Hong Kong Polytechnic University, Hong Kong

HIGHLIGHTS

- In-house model of easy-to-tune operation strategy for solar tower power is developed.
- Five operational thresholds affecting the power generation are identified.
- Holism-based rolling optimization to enhance particle swarm optimization is proposed.
- Operation strategy is optimized by above methods with future irradiation conditions.
- The average daily power production is increased by 13.4%.

ARTICLE INFO

ABSTRACT

Solar tower power plants (STP) with thermal energy storage have the ability to temporally shift power generation, regulate peak load and modulate frequency. The power production of such systems not only depends on the available solar resources, but also on the operation strategies, such as the operational thresholds used to control when the equipment starts or stops in certain conditions. Currently, most of the operational thresholds are determined by operators' experience or the rated parameters given by the equipment manufacturers, which are usually unoptimized fixed values. Therefore, to guide the optimal operations of STP, optimization methods are developed in this work to optimize the daily operational thresholds according to the solar radiation at present and in the future. Firstly, a well-validated in-house model with easy-to-tune operation strategies for STP is developed to optimize the thresholds. Then, five operational thresholds affecting the power generation of STP are identified. Finally, an optimization algorithm is proposed to optimize the operational thresholds. The proposed optimization algorithm uses a rolling optimization based on holism to enhance regular particle swarm optimization (R-PSO). The power generation of a 50 MW STP under three different operation strategies is compared: (1) unoptimized operation strategy, (2) operation strategy optimized by regular PSO algorithm, and (3) operation strategy optimized by R-PSO algorithm. The average daily power generation under the three operation strategies is 451.16 MWh, 490.25 MWh, and 511.63 MWh, respectively. The results show that the proposed R-PSO could increase averaged daily power production by 13.4 % and 4.36 % when compared with cases with no optimization and PSO optimization, respectively. Therefore, the power production of STP can be significantly improved by optimizing the identified daily operational thresholds using the R-PSO algorithm.

Nomenclature		h_{mixed}	Mixed convection heat-transfer coefficient (W/(m^2·K))
		k	Heat transfer coefficient (W/(m^2·K))
Symbol	**Name (Unit)**	k_{film}	Air conductivity (W/(m·K))
A	Area (m^2)	l	Length (m)
D	Diameter (m)	R	Climbing capacity (W)
DNI	Direct normal irradiance (W/m^2)	r	Radius (m)
H	Height (m)	T	Temperature (°C)
L	Molten salt liquid level in the tank (m)	P	Power (W)
M	Quality(kg)	$\dot{m}$	Mass flow rate (kg/s)
N	Number	$\dot{Q}$	Thermal power (W)
Q	Thermal energy(J)	t	Time (s)
Nu	Nusselt number	U_t	The total heat transfer coefficient (W/(m^2·K))
c	Specific heat capacity (J/(kg·K))	η	Efficiency
h	Enthalpy (J)	Δ	Interval
h_{for}	Forced convection heat-transfer coefficient (W/(m^2·K))	ρ	Density (kg/m^3)
h_{nat}	Natural convection heat-transfer coefficient (W/(m^2·K))		

1. Introduction

To reduce pollution and mitigate climate change, renewable energy sources (especially solar and wind energy) are replacing fossil fuels globally in power production [1,2]. Due to the intermittent nature of solar and wind resources, some measures are taken to mitigate the temporal variability for those power productions. Concentrated solar power (CSP) plants with thermal energy storage (TES) have the ability to temporally shift power generation, regulate peak and modulate frequency [3–5]. Solar tower power (STP) is one major form of CSP. In STP system, solar radiation is reflected by the heliostat field and concentrated on the receiver to heat the working fluid. The working fluid then exchanges heat with water in a heat exchanger to produce superheat steam, then the steam drives turbine for power generation. The excess heated working fluid is stored in the TES module.

Once a CSP plant is built and operating, the design parameters are fixed and cannot be changed. During operation, the operational thresholds of the plant can be adjusted to change power output. For STP, operational thresholds refer to the parameters that control when the equipment starts or stops, such as the direct normal irradiation (DNI) for the receiver to start operating, and the liquid level in storage tanks for the turbine to start or stop operating. Currently, most of the thresholds are determined according to engineers' experience or provided by the equipment manufacturer, which are preset without any optimization. As such, most of the plants are not operating in the optimal conditions to generate the maximum possible power. Therefore, this work aims at performing optimization of the operational thresholds to increase the power generation of existing STP plants. To optimize the operational thresholds, an accurate and easy-to-tune power plant model and an appropriate optimization method are needed.

At present, most researchers have studied single-module models of STP plants, such as the models for the heliostat field and the receiver. Besarati et al. [6] established a heliostat field model with high computational efficiency, which significantly shortened the calculation time of shadowing and blocking efficiency. Piroozmand et al. [7] established a mathematical model of multi-tower heliostat field and introduced a method to improve the optical properties and annual efficiency of the heliostat field. Rodríguez-Sánchez et al. [8] established a detailed receiver model of STP plant considering the circumferential temperature variations, and calculated the radiation loss and thermal efficiency in the receiver. Luo et al [9] studied the model of a novel dual-receiver that improved the thermal efficiency of STP plant. A few researchers have established the system models of STP plants. For example, Wang et al. [10] established a model of the heliostat field and receiver, where STP power production is forecasted by integrating physical modeling with deep learning techniques. Benammar et al. [11] established a general nonlinear mathematical model of STP plant without thermal storage module, which mainly includes heliostat field subsystem, cavity receiver subsystem, steam generation subsystem, and Rankine cycle subsystem. Xu et al. [12] established a theoretical model of molten salt STP plant, in which a modified thermal model for the molten salt cavity receiver is proposed. System Advisor Model (SAM) is a widely-used software for STP systems developed by the Renewable Energy Laboratory of the United States, which can calculate variables such as power generation and the capacity factor of STP plant [13]. However, the operation strategy in SAM software is greatly simplified, i.e. each weekday in one month shares the same strategy, and only the steam turbine output can be adjusted. All of the forementioned models in the literature don't have the mechanism to improve the operation strategy by optimizing operational thresholds adaptively according to the actual solar radiation data, thus not suitable for operational threshold optimization to achieve the maximal amount of annual electricity generation.

In the research of STP plant optimization, the design parameters are mainly optimized, which include the heliostat field layout, the duration of TES, design DNI, and solar multiple (SM). Saghafifar et al. [14] optimized the heliostat field with the objective function of field efficiency and levelized cost of energy (LCOE) using the Analysis of Implementation of Non-Equal Heliostats (AINEH) algorithm. Marugán-Cruz et al. [15] studied the optimal SM of direct steam generation (DSG) linear Fresnel plant without thermal storage, while the optimization objective is to minimize LCOE. Lee et al. [16] optimized the heliostat field layout using the Genetic Algorithm (GA). Atif et al. [17] established a mathematical model for optimizing the heliostat field layout using the Differential Evolution algorithm (DE), and calculated heliostat field efficiency at each stage of the optimization. Khosravi et al. [18] trained the neural network using the calculation results of the SAM, then a combined optimization algorithm is used to optimize the design parameters under different longitude and latitude. However, the operational thresholds in operation strategy are not optimized in all the above literature and no suitable optimization methods are proposed.

For holistic optimization, it can be classified as whole system-based type and time span-based type. In the area of solar energy applications, most of the research are whole system-based optimization. Alirahmi et al. [19] proposed a multi-generation system with geothermal energy and parabolic trough solar collectors, to simultaneous generation of power, cooling, freshwater, hydrogen, and heat. A multi-objective optimization genetic algorithm was used to improve the whole system performance. Zhang et al. [20] proposed a simulated annealing algorithm-based chaotic search and harmony search algorithm for modeling and optimally sizing a hybrid system for renewable energy (wind and solar). Two storage device options were considered: chemical storage via hydrogen and electrochemical storage via batteries.

Regarding the few time span-based optimization schemes, Mayer et al. [21] optimized the hybrid renewable energy systems (HRES) based on full life-cycle for the first time, with the objective function of minimizing the environmental footprint and the net present cost. The importance of life-cycle assessment in the HRES design was proved, and a framework for practical applications was provided.

As annual power generation is one of the most important indicators to evaluate the overall performance of STP power plants in China [22], there is still a lack of whole-system optimization based on the full-year time span in the research of STP plants. To fill the above research gap, a minute-wise STP model with adjustable operation strategy embracing all operating modes is firstly developed. The relationship between the operational thresholds and the power generation is then analyzed to identify decision variables that affect the power generation. Considering the operation safety of each module, the constraint conditions of the STP model are established. The annual power generation is selected as the objective function to be maximized, and the rolling optimization based on holism enhanced particle swarm optimization algorithm (R-PSO) is proposed for threshold optimization. Varying solar radiation resources are fed into the R-PSO to obtain daily optimal values of the operational thresholds. The power output from the proposed R-PSO is then compared with the counterpart without optimization and with only particle swarm optimization (PSO) to demonstrate the benefits of the proposed methodology.

2. Mathematical model of solar tower power system

The modeling of the STP plant includes (1) heliostat field subsystem; (2) molten salt cycle subsystem (receiver, TES, upper and lower salt pipes); (3) Rankine cycle subsystem (heat exchanger, main steam pipe, steam turbine, and condenser) and (4) the operation strategy.

In the following subsections, the main models are presented briefly for the heliostat field, the receiver, the TES, and the heat exchanger. The other models are similar to those in traditional thermal power plants thus will not be presented here for conciseness. The complete STP modeling software developed and used here is named as the Performance Evaluation for Solar tower power plants (PES).

The simplified scheme of the STP plant model is shown in Fig. 1. In the molten salt cycle subsystem, the red line represents the flow path of hot salt while the blue line represents the flow path of cold salt. The scheme shown in Fig. 1 is more similar to actual power plants when

compared with the scheme in SAM [23].

2.1. The model of the heliostat field

As the detailed calculation of the heliostat field has been described in Ref. [24–27] published by the authors, the model of the heliostat field is only briefly summarized here.

The optical efficiency of each heliostat at any time is:

$$\eta_{opt} = \eta_{ref}\eta_{cos}\eta_{atm}\eta_{sb} \tag{1}$$

where η_{opt} is the instantaneous optical efficiency of the heliostat; η_{ref} is the instantaneous reflection efficiency; η_{cos} is the cosine efficiency, i.e., the cosine value of the angle between the incident light and the surface normal direction of the heliostat; η_{atm} is the atmospheric attenuation efficiency, which is caused by atmospheric absorption, scattering and reflection, and calculated by the formula proposed by Biggs et al. [28]; η_{sb} is the shadowing and blocking efficiency, which is calculated using the geometric projection method proposed by Sassi [29].

The instantaneous optical efficiency of the heliostat field is:

$$\eta_{hf} = \frac{\sum_{i=1}^{n}\eta_{opt}}{n} \tag{2}$$

where n is the number of heliostats; η_{hf} is the instantaneous optical efficiency of the heliostat field.

The solar flux on a heliostat is:

$$\dot{Q}_h = DNI\eta_{opt}A_h \tag{3}$$

where DNI [W/m^2] is the direct normal irradiance; and A_h [m^2] is the area of the heliostat. The incident solar flux on the receiver surface directed by the heliostat is:

$$\dot{Q}_{rx} = \frac{\dot{Q}_h \cdot \cos\varphi}{\pi r^2} \tag{4}$$

where φ [rad] is the angle between the reflected radiation from the heliostat and the corresponding normal direction of the receiver; and r [m] is the radius of the spot reflected by the heliostat on the surface perpendicular to the reflected radiation through the central point of the receiver:

$$r = \tan a \cdot l \tag{5}$$

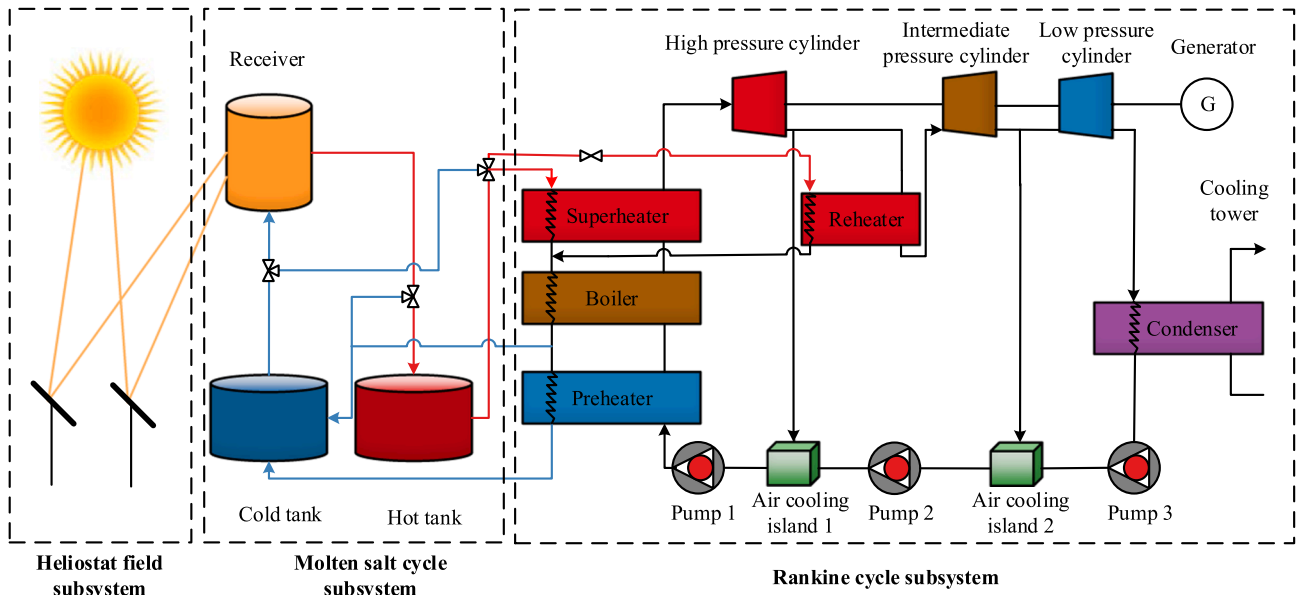**Fig. 1.** The modeled STP plant.

where a = 4.65 mrad is the half-angle of the direct solar radiation reaching the earth's surface; and l [m] is the distance between the heliostat center point to the receiver center point.

The energy flux distribution on the receiver is superposed by the reflected solar flux from all the heliostats. Based on the methods of energy superposition and rotating transition of coordinate, the energy flux of each point on the receiver surface is calculated, and repeated calculations could give the energy flux distribution of the entire receiver [27,30].

2.2. The model of the receiver

The cylindrical surface of the receiver is composed of a large number of rectangular panels, and each panel is composed of collector tubes. The working fluid (molten salt is used) in the receiver is heated by absorbing the solar heat, with the flow path shown in Fig. 2. The pressure resistance loss of the receiver includes the resistance of the straight pipe section and the resistance of the 90° elbow pipe on each panel, as detailed in [23].

Equations (6)-(8) are used to calculate the forced, natural, and mixed convection coefficients between the receiver and the surrounding air. Equation (9) uses Newton's law of cooling to obtain the convective loss of the i th panel. Equation (10) calculates the total convective loss of the receiver.

$$h_{\text{for}} = \text{Nu}_{\text{for}} k_{\text{film}} / D_{\text{rx}} \tag{6}$$

$$h_{\text{nat}} = \text{Nu}_{\text{nat}} k_{\text{film}} / H_{\text{rx}} \tag{7}$$

$$h_{\text{mixed}} = \left(h_{\text{for}}^m + h_{\text{nat}}^m \right)^{1/m} \tag{8}$$

$$\dot{Q}_{\text{conv}}(i) = h_{\text{mixed}} A_{\text{pnl}} \left(T_{\text{pnl}}(i) - T_{\text{amb}} \right) \tag{9}$$

$$\dot{Q}_{\text{conv,sum}} = \sum_{i=1}^{N_{\text{pnl}}} \dot{Q}_{\text{conv}}(i) \tag{10}$$

where h_{for}, h_{nat} and h_{mixed} [W/(m^2·K)] are the forced, natural, and mixed convection coefficients; Nu_{for} and Nu_{nat} are the Nusselt number of forced and natural convection, respectively; k_{film} [W/(m·K)] is the thermal conductivity of air; D_{rx} and H_{rx} [m] are the diameter and height of the receiver; $\dot{Q}_{\text{conv}}$ [W] is the convective losses from each panel; A_{pnl} [m^2] is the area of each panel; T_{pnl} [K] is the average temperature of each panel; T_{amb} [K] is the ambient temperature; $\dot{Q}_{\text{conv,sum}}$ [W] is the total convective loss; and N_{pnl} is the number of panels.

Regarding to radiative heat loss to the surroundings, Equations (11)-(13) describe the environmental radiation coefficient, environmental radiation heat loss, sky radiation coefficient and sky radiation heat loss.
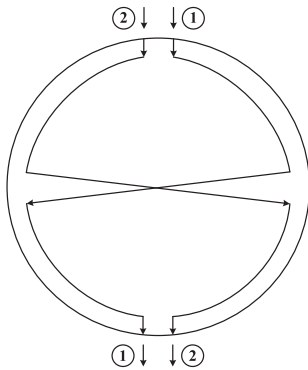
Equations (14)-(16) are used to calculate the radiative losses of receiver.

$$h_{\text{rad,amb}}(i) = \sigma \varepsilon F_{\text{s,amb}} \left(T_{\text{pnl}}^2(i) + T_{\text{amb}}^2 \right) \left(T_{\text{pnl}}(i) + T_{\text{amb}} \right) \tag{11}$$

$$\dot{Q}_{\text{amb}}(i) = h_{\text{rad,amb}}(i) A_{\text{pnl}} (T_{\text{pnl}}(i) - T_{\text{amb}}) \tag{12}$$

$$h_{\text{rad,sky}}(i) = \sigma \varepsilon F_{\text{s,sky}} \left(T_{\text{pnl}}^2(i) + T_{\text{sky}}^2 \right) \left(T_{\text{pnl}}(i) + T_{\text{sky}} \right) \tag{13}$$

$$\dot{Q}_{\text{sky}}(i) = h_{\text{rad,sky}}(i) A_{\text{pnl}} (T_{\text{pnl}}(i) - T_{\text{amb}}) \tag{14}$$

$$\dot{Q}_{\text{rad}}(i) = \dot{Q}_{\text{amb}}(i) + \dot{Q}_{\text{sky}}(i) \tag{15}$$

$$\dot{Q}_{\text{rad,sum}} = \sum_{i=1}^{N_{\text{pnl}}} \dot{Q}_{\text{rad}}(i) \tag{16}$$

where $h_{\text{rad,amb}}$ and $h_{\text{rad,sky}}$ [W/m^2·K] are environment radiation coefficient and sky radiation coefficient respectively; σ= 5.67×10^{-8} W/m^2·K^4 is the Stefan-Boltzmann constant; ε is the surface emittance of the receiver; $F_{\text{s,amb}}$ and $F_{\text{s,sky}}$ are view factors from the receiver to the ambient and from the receiver to sky, respectively; and T_{sky} [K] is equivalent sky temperature. $\dot{Q}_{\text{amb}}$ and $\dot{Q}_{\text{sky}}$ [W] are the radiative loss from each panel to the ambient and to the sky, respectively; $\dot{Q}_{\text{rad}}$ [W] is the total radiative loss from each panel; and $\dot{Q}_{\text{rad,sum}}$ [W] is the total radiative loss from the receiver.

According to surface energy balance, the heat absorbed by each panel is calculated by Equation (17). Equation (18) is used to calculate the working fluid's temperature at the outlet of each panel. Since the receiver has two flow paths, Equations (19)-(20) are used to calculate the mixing temperature, and the thermal power at the outlet of the receiver, respectively [8,11].

$$\dot{Q}_{\text{abs}} = \dot{Q}_{\text{inc}} - \dot{Q}_{\text{conv,sum}} - \dot{Q}_{\text{rad,sum}} \tag{17}$$

$$T_{\text{pnl,o}}(i) = T_{\text{pnl,i}}(i) + \dot{Q}_{\text{abs}}(i) / \left[c_{\text{pnl,s}}(i) \dot{m}_{\text{rx,o}} / 2 \right] \tag{18}$$

$$\overline{T}_{\text{rx,o}} = \frac{1}{2} \left(T_{\text{pnl,o}} \left(N_{\text{pnl}} / 2 \right) + T_{\text{pnl,o}} \left((N_{\text{pnl}} + 1) / 2 \right) \right) \tag{19}$$

$$\dot{Q}_{\text{rx,o}} = \dot{m}_{\text{rx,o}} c_{\text{pnl,salt}} \left(\overline{T}_{\text{rx,o}} - \overline{T}_{\text{rx,i}} \right) \tag{20}$$

where $\dot{Q}_{\text{abs}}$ [W] is the heat absorbed by each panel; $\dot{Q}_{\text{inc}}$ [W] is the incident solar power on each panel; $T_{\text{pnl,i}}$ and $T_{\text{pnl,o}}$ [K] are the molten salt temperature at the inlet and outlet of the panel. $\dot{m}_{\text{rx,o}}$ [kg/s] is the mass flow rate of the salt in the receiver; $c_{\text{pnl,salt}}$ [J/kg·K] is the specific heat capacity of the molten salt in the panel; $\overline{T}_{\text{rx,o}}$ [K] is the salt temperature at the outlet of the receiver; $T_{\text{pnl,o}} \left(N_p / 2 \right)$ and $T_{\text{pnl,o}} \left((N_p + 1) / 2 \right)$ [K] are the salt temperature of the outlets of two flow paths; $c_{\text{pnl,salt}}$ [J/kg·K] is the average specific heat capacity of molten salt in the receiver; $\overline{T}_{\text{rx,i}}$ [K] is the salt temperature at the inlet of receiver; $\dot{Q}_{\text{rx,o}}$ [W] is the output thermal power of the receiver.

Equation (21) is used to calculate the thermal efficiency of receiver.

$$\eta_{\text{rx}} = \frac{\dot{Q}_{\text{rx,o}}}{\dot{Q}_{\text{hf}}} \tag{21}$$

2.3. The model of the thermal energy storage system

The TES system includes a cold salt tank and a hot salt tank, and the mathematical models of two tanks are similar. After meeting the corresponding thermal power demand of the steam turbine, the remaining hot salt from the receiver is stored in the hot tank, and the cold salt after used by the heat exchanger is stored in the cold tank.

According to mass and energy conservations, the mass flow rate and

Fig. 2. The flow path of the working fluid in the receiver, vertical view. The working fluid flows in from the north of receiver in two ways: crosses in the east–west direction and flows out from the south.

temperature of the molten salt in the tank at the current time are calculated using Equations (22)-(23). The heat loss from the tank to the surroundings is calculated by Equation (24). The liquid level of the molten salt in the tank is calculated by Equation (25).

$$\frac{dM_s}{dt} = \dot{m}_{s,i} - \dot{m}_{s,o} \tag{22}$$

$$c_s \frac{d(M_s T_s)}{dt} = \dot{m}_{s,i} h_{s,i} - \dot{m}_{s,o} h_{s,o} - \dot{Q}_{loss} \tag{23}$$

$$\dot{Q}_{loss} = U_t (T_s - T_{amb}) \tag{24}$$

$$L_s = M_s / \left(\rho_s \pi (D_s/2)^2 \right) \tag{25}$$

where M_s [kg] is the total mass of molten salt in each tank; $\dot{m}_{s,i}$ and $\dot{m}_{s,o}$ [kg/s] are the mass flow rate at the inlet and outlet of tank, respectively; T_s [K] is the temperature of the molten salt in each tank; $h_{s,i}$ and $h_{s,o}$ [J/kg] are the enthalpy of molten salt at the tank inlet and outlet; $\dot{Q}_{loss}$ [W] is the heat loss from the tank to surroundings; U_t [W/m^2·K] is the total heat transfer coefficient between the tank and its surroundings, which considers the heat loss from both salt-filled portion of the tank and the empty portion of the tank [31]. L_s [m] is the liquid level of molten salt in the tank; ρ_s [kg/m^3] is the density of molten salt; and D_s [m] is the diameter of tank.

2.4. The model of the heat exchanger

As shown in Fig. 3, the heat exchanger system includes a preheater, a boiler, a superheater, and a reheater. Feed water is pumped into the preheater and heated up to a temperature that approaches the saturation temperature. Preheated water is then being heated to saturated steam in the boiler and to superheated steam in the superheater before entering the turbine. The steam at the outlet of the high-pressure cylinder is reheated by the reheater before entering the intermediate pressure cylinder. To control the salt temperatures at the inlets of the superheater and the reheater, the hot and cold salt are mixed before entering to the superheater and the reheater. To control the salt temperature in the preheater, a part of the molten salt is extracted from the outlet of the boiler. Counterflow scheme is adopted to exchange heat between the molten salt and the water/steam.

Equations (26)-(31) are used to quantify the heat transfer processes between salt and water in the superheater, energy conservation law and the average temperature difference method [32,33] are used.

$$\dot{Q}_{sup} = \dot{m}_{sup,w} \left(c_{sup,w,o} T_{sup,w,o} - c_{sup,w,i} T_{sup,w,i} \right) \tag{26}$$

$$\dot{Q}_{sup} = \dot{m}_{sup,s} \left(c_{sup,s,o} T_{sup,s,o} - c_{sup,s,i} T_{sup,s,i} \right) \eta_{ex,sup} \tag{27}$$

$$\dot{Q}_{sup} = k A_{sup} \Delta T_m \tag{28}$$

$$\Delta T_m = \frac{\Delta T_{max} - \Delta T_{min}}{ln \frac{\Delta T_{max}}{\Delta T_{min}}} \tag{29}$$

$$\Delta T_{max} = T_{sup,s,i} - T_{sup,w,o} \tag{30}$$

$$\Delta T_{min} = T_{sup,s,o} - T_{sup,w,i} \tag{31}$$

where $\dot{Q}_{sup}$ [W] is the thermal power absorbed by steam in the superheater; $T_{sup,s,o}$ and $T_{sup,s,i}$ [K] are the salt temperatures at the outlet and inlet of the superheater, respectively; $T_{sup,w,o}$ and $T_{sup,w,i}$ [K] are the steam temperatures at the outlet and inlet of the superheater, respectively; $c_{sup,w,o}, c_{sup,w,i}, c_{sup,s,o}$ and $c_{sup,s,i}$ [J/kg·K] are the specific heat capacity of water and salt at the inlet and outlet of the superheater, respectively; $\dot{m}_{sup,w}$ and $\dot{m}_{sup,s}$ [kg/s] are the mass flow rate of water and salt in the superheater, respectively; $\eta_{ex,sup}$ is the heat transfer efficiency of the superheater; k [W/m^2·K] is the overall heat transfer coefficient between salt and water; and A_{sup} [m^2] is the heat transfer area.

Equations (32)-(33) calculate the mass flow rate and enthalpy of molten salt at the inlet of superheater.

$$\dot{m}_{sup,s,cld,i} + \dot{m}_{sup,s,hot,i} = \dot{m}_{sup,s,i} \tag{32}$$

$$\dot{m}_{sup,s,cld,i} h_{sup,s,cld,i} + \dot{m}_{sup,s,hot,i} h_{sup,s,hot,i} = \dot{m}_{sup,s,i} h_{sup,s,i} \tag{33}$$

where $\dot{m}_{sup,s,cld,i}$, $\dot{m}_{sup,s,hot,i}$ [kg/s], $h_{sup,s,cld,i}$ and $h_{sup,s,hot,i}$ [J/kg] are the mass flow rate and enthalpy of cold salt and hot salt at the inlet of superheater, respectively. $h_{sup,s,i}$ [J/kg] is the enthalpy of molten salt after cold salt and hot salt are mixed at the inlet of superheater.

The calculation methods of the reheater and preheater are the same as the superheater. Equations (34)-(35) describe the heat transfer process in the boiler.

$$\dot{Q}_b = \dot{m}_{b,s} \left(c_{blr,s,o} T_{blr,s,o} - c_{blr,s,i} T_{blr,ss,i} \right) \eta_{ex,blr} \tag{34}$$

$$\dot{Q}_{blr} = \dot{m}_{blr,w} \left(c_{blr,w,o} T_{blr,w,o} - c_{blr,w,i} T_{blr,w,i} \right) \tag{35}$$

where $\dot{Q}_{blr}$ [W] is the thermal power absorbed by water in the boiler; $\dot{m}_{blr,s}$ and $\dot{m}_{blr,w}$ [kg/s] are the mass flow rate of molten salt and water
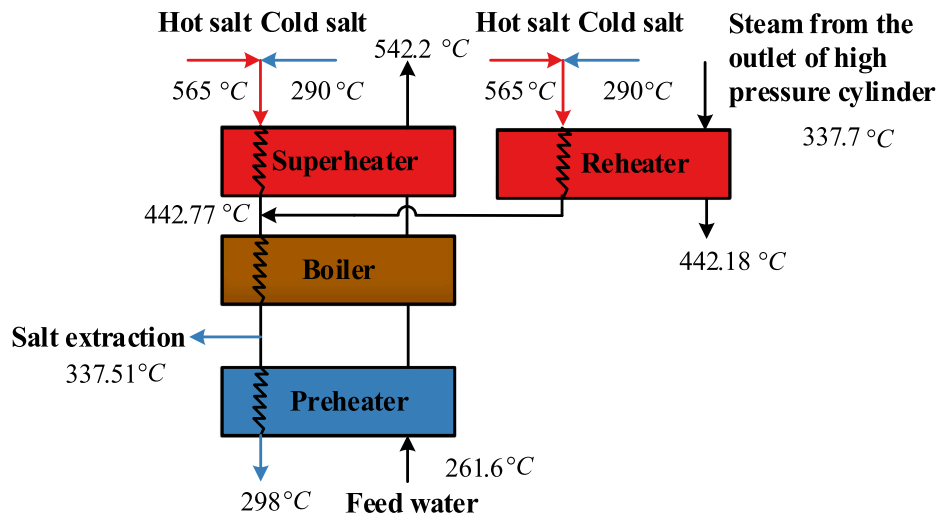

Fig. 3. The heat exchanger system.

in the boiler, respectively; $c_{blr,w,o}$, $c_{blr,w,i}$, $c_{blr,s,o}$ and $c_{blr,s,i}$ [J/kg K] are the specific heat capacity of water and salt at the inlet and outlet of boiler respectively; $T_{blr,s,o}$, $T_{blr,s,i}$, $T_{blr,w,o}$ and $T_{blr,w,i}$ [K] are the temperature of molten salt and water at the inlet and outlet of the boiler respectively; $\eta_{ex,blr}$ is the heat transfer efficiency of the boiler.

Equation (36) calculates the mass flow rate of salt extracted from the outlet of the boiler.

$$\dot{m}_{blr,sob} = \dot{m}_{blr,s} - \dot{m}_{pre,s} \qquad (36)$$

where $\dot{m}_{blr,sob}$ [kg/s] is the mass flow rate of molten salt extracted from the outlet of the boiler; and $\dot{m}_{pre,s}$ [kg/s] is the mass flow rate of molten

salt in the preheater.

2.5. Operation strategy

The operation strategy of the STP plant is shown in Fig. 4. In this work, the operation strategy of the receiver is shown as the main axis, and the operation stages (opening, preheating, feeding salt, heating operation, normal operation, draining salt and shutdown) of the receiver are determined according to the operational parameters (current DNI, future DNI and the molten salt temperature in receiver). The inlet and outlet salt temperature, mass flow rate, and other parameters of the receiver are calculated.
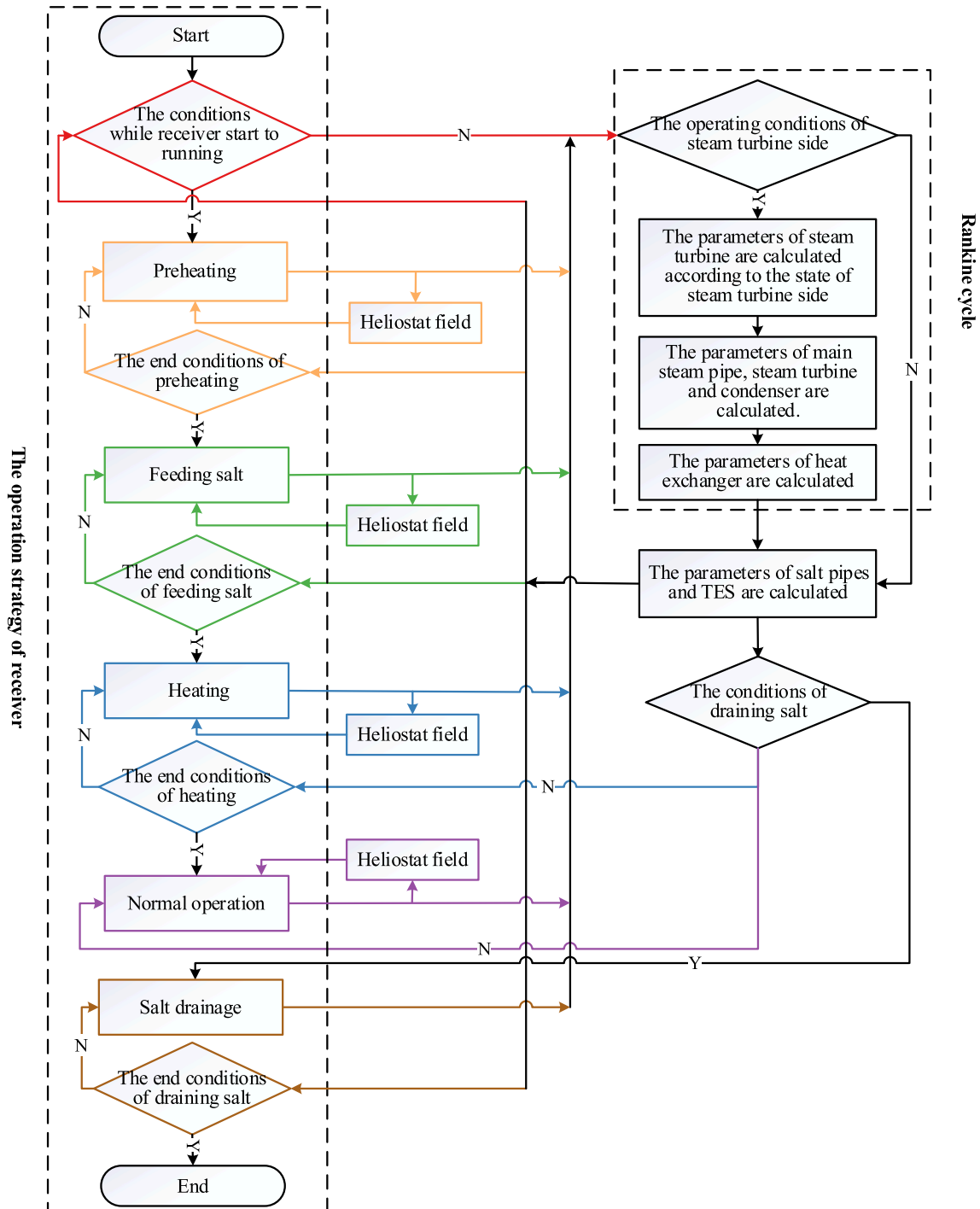

Fig. 4. The operation strategy of the STP plant.

The operation conditions of the heliostat field, Rankine cycle, and the TES system are determined according to the operation mode of the receiver. If the receiver needs solar heat provided by the heliostat field and the heliostat field can work normally, the actual projected energy of the heliostat field can be calculated. The energy obtained by the receiver is determined according to its operation stage and the maximum received energy. The operation condition of TES is determined according to the mass flow rate at the inlet and outlet of the receiver and the heat exchanger, while the operation condition of the salt pipes is determined by the mass flow at the inlet and outlet of the receiver and TES. The minimum operating liquid level of the cold tank, current DNI, and future DNI determine whether the receiver should start draining salt and shut down. Furthermore, the minimum operating liquid level of the hot tank determines whether the steam turbine is ready to reduce load and shut down. The operation conditions of the steam turbine and condenser are decided according to the energy provided by the receiver and TES. The operation of heat exchanger, main steam pipe, and condenser are accompanied by the operation of the steam turbines.

The red, yellow, green, blue, purple, and brown color lines in Fig. 4 indicate the operation strategies when the receiver is in the operation stages of start, preheating, feeding salt, heating, normal, and draining salt condition, respectively. The dotted line box on the left shows the operation strategy of the receiver, and the dotted line box on the right represents the operation strategy of Rankine cycle.

2.6. Model validation

In this work, the module models of heliostat field, receiver, TES, heat exchanger, steam turbine, and condenser are developed. The operation of each module is scheduled according to the operation strategy. The calculation program is written in MATLAB (2017A) using its dynamic link library. The PES software is developed in Java. At present, PES is in the stage of practical application and verification.

The molten salt is composed of 60 % sodium nitrate and 40 % potassium nitrate. The measured 1-min averaged DNI values over one year in Northwest China are shown in Fig. 5, and the specifics of the STP plant are shown in Table 1. The measured irradiation data in Northwest China is also used for the optimization of operational thresholds. The annual total power generation calculated by PES is 177,062 MWh, and the value calculated by SAM software is 179,890 MWh, with 1.57 % difference. The monthly power generation calculated by PES and SAM are shown in Fig. 6, indicating that the average difference between the two models is less than 3.9 %. The comparisons of hourly power generation in four typical days are plotted in Fig. 7, where two models produce similar results. As such, the module models and operation strategy models of PES are validated.
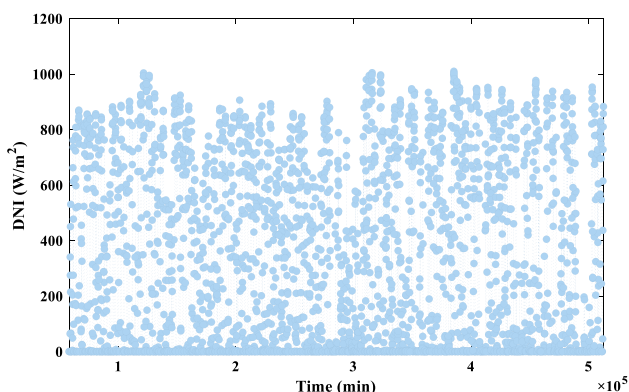
Table 1
The specifics of the STP plant.

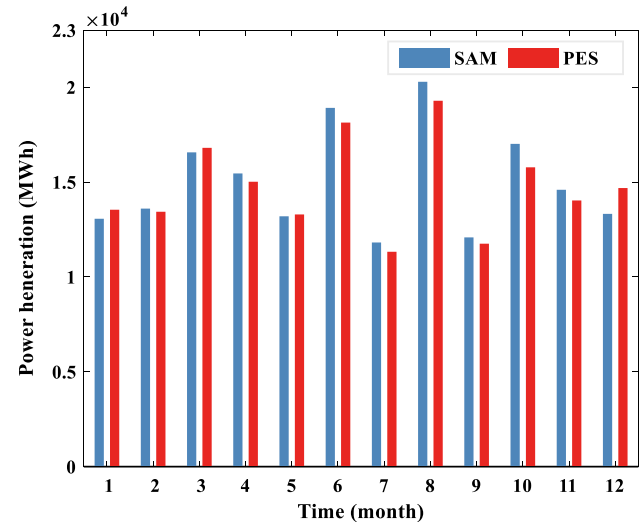| Items	Average annual radiation	Installed capacity	TES hours	Solar multiple	Area of each heliostat	Number of heliostats
Value	1900 kWh/m²/a	50 MW	6 h	1.8	20 m²	25,795

Fig. 6. Comparisons of monthly power generation.

2.7. Comparison of developed model with commercial software

PES is an in-house model of molten salt solar tower power plant with an easy-to-tune operation strategy. To calculate minute-wise STP output for one year (525600 points in total), the total computing time without optimization algorithm is about 4 h on a computer with 8 GB RAM and Intel Core i5-104000 CPU @ 2.90 GHz.

As presented in Table 2, PES has several characteristics that made it more suitable for threshold optimization when compared with SAM. Therefore, the optimization studies presented in Sections 3, 4, and 5 are based on PES.

3. Effects of the operational thresholds on power generation

According to the analysis of system operation strategy, the daily power generation and its trend are affected by (a) the liquid levels in cold and hot tanks for the receiver and steam turbine to start reducing load, (b) the operation strategy of the receiver, as well as (c) the operational thresholds in each stage of the receiver and the steam turbine. The power generation profile will change when operational thresholds are adjusted.

In this section, the DNI data of the first month in Fig. 5 are used to quantify the effects of some operational thresholds on power generation, as shown in Fig. 8. The selected operational thresholds are:

Parameter 1: the liquid level in hot tank for the steam turbine to start reducing load and shutdown, $L_{v,hf}$;

Parameter 2: the liquid level in cold tank for the receiver to start draining salt, L_{cld};

Parameter 3: the DNI level for the receiver to start operating, DNI_{start};

Parameter 4: the minutes before sunset for the receiver to be able to start operating, t_{sunset};

Parameter 5: the critical value of the molten salt temperature when entering the hot and cold tanks, T_{cs};

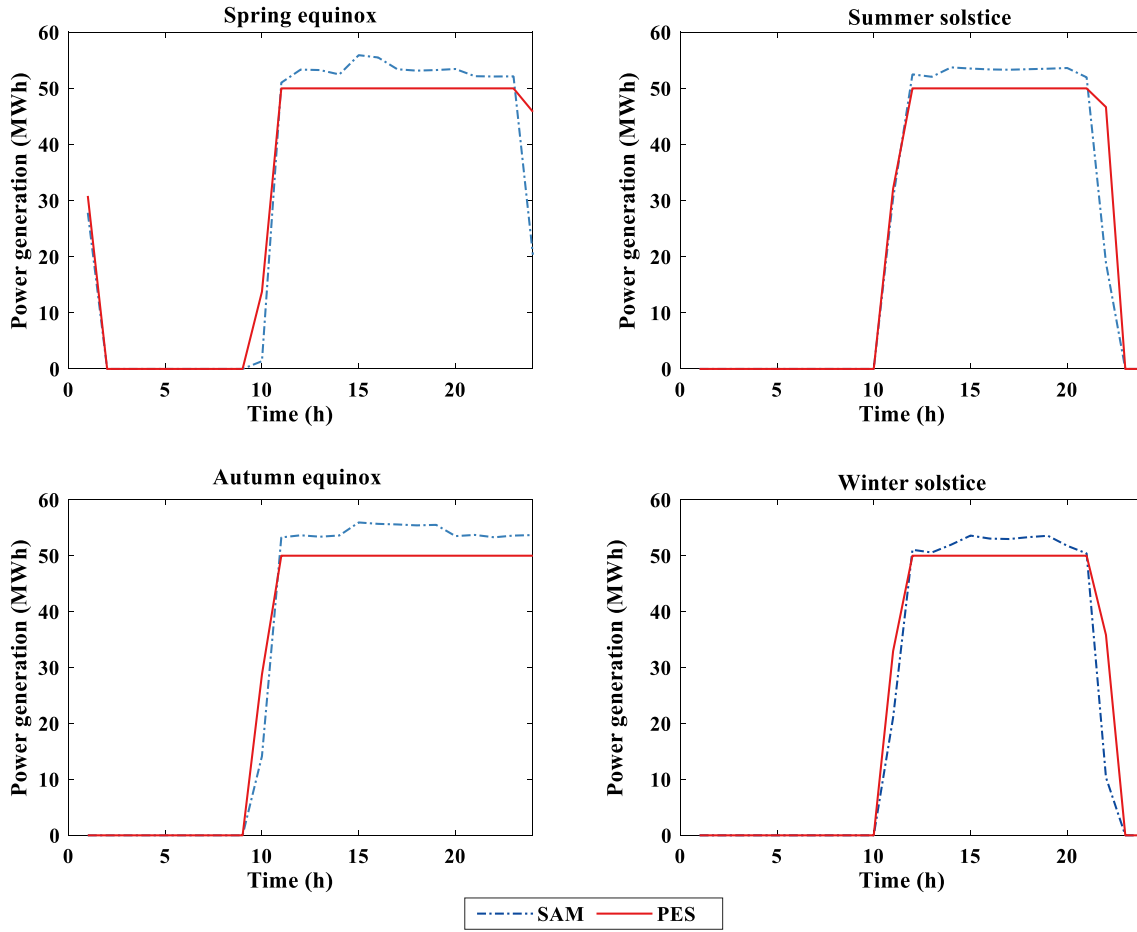Parameter 6: the DNI level for the receiver to start feeding

Fig. 5. The 1-min averaged DNI measurements over the year 2019.

Fig. 7. Comparisons of power generation profiles in selected days.

salt,DNI$_{insalt}$;

Parameter 7: the molten salt temperature for the receiver to start normal operation,T_{rx}.

Fig. 8 shows that parameters 1, 2, 3, 4, and 6 have great effects on power generation which belong to quasi-concave functions in game theory; while parameters 5 and 7 don't meet the definition.

4. Optimization model

Operational thresholds Parameter 1, 2, 3, 4, and 6 are selected as decision variables to maximize power generation in the following sections [34]. The maximum power generation of each optimization stage is the objective function.

4.1. Objective function

The objective function of the k th optimization is:

$$f(k) = \text{maximize}\left\{\sum_{i=k}^{k+l-1} W(L_{\text{hot}}(i), L_{\text{cld}}(i), \text{DNI}_{\text{start}}(i), t_{\text{sunset}}(i), \text{DNI}_{\text{insalt}}(i))\right\} \quad k$$

$$= 1, 2, 3 \ldots, n \tag{37}$$

where l is the optimization length, which is determined by solar radiation data, generally $l = 2$ or 3 days according to the TES capacity; W is the daily power generation, kWh; and n is the total number of optimization days.

4.2. Rolling optimization based on holism improved particle swarm optimization

The selected decision variables are affected by the current and future meteorological variables, including DNI, air temperature, wind speed, etc. For example, if solar radiation is sufficient in the next day, a certain amount of hot salt may be left in the hot tank for preheating the steam turbine in the morning of the next day. The purpose of rolling optimization based on holism improved the particle swarm optimization (R-PSO) is to use holism in decision-making scenarios, that is, subordinate immediate interests to long-term interests, and subordinate partial interests to overall interests. R-PSO is believed to be able to break through the bottleneck of increasing the optimization effect simply from the perspective of improving mathematical-based approaches. To overcome the disadvantages of PSO algorithm, the control parameters (inertia weight, learning factors) were optimally selected by trial and error. To be specific, preliminary repeated experiments with different PSO control parameters were conducted, and the parameters yielding the best global exploration ability as well as the maximum/minimum fitness value were selected in order to avoid the local optimal problem. The optimization procedure of R-PSO is:

(1) Minute-wise irradiation data in the $(n + l - 1)$ days are obtained and the initial liquid levels in hot and cold tanks are set.

(2) In the k th optimization, the optimization time is from Day k to Day $k + l - 1$. If $k = 1$, the liquid levels in the cold and hot tanks are the initial liquid levels mentioned in (1). When $k \geqslant 2$, the liquid levels at the end of the $(k - 1)$ th day obtained from the $(k - 1)$ th optimization are used. Moreover, the solar radiation data from Day k to Day $k + l - 1$ are used.

Table 2
Comparisons between PES and SAM.

Models	PES	SAM [23]
Heliostat field	The field layout optimization is based on mutation differential evolution.	Radially staggered method of field layout.
Receiver	The detailed model of the receiver is established, including the stages of start, preheating, feeding salt, heating, normal and draining salt.	The model only has a normal operation stage.
Thermal energy storage	The heat loss from the tank to the environment is calculated every minute considering changing solar radiation.	Not considered.
Heat exchanger	The model is more suitable for engineering practices. (a) The model of reheater is added; (b) The salt pumped into the superheater and the reheater is the mixture of hot and cold salt; (c) A part of the molten salt is extracted from the outlet of boiler.	(a) No reheater; (b) No mixtures of hot and cold salt; (c) The salt from the outlet of the boiler isn't extracted.
Steam turbine	(a) The efficiency and power production of each cylinder are calculated through iterations; (b) The eight-stage extraction turbine model is developed.	(a) The efficiency of each cylinder is given and fixed; (b) Two stage extraction turbine model is used.
Pipeline	The models of up flowed salt pipe, down flowed salt pipe and main steam pipe are developed.	Not modeled.
Operation strategy	The scheduling strategy for each module is adaptive. The calculation interval is one minute.	The scheduling strategy of each weekday in a month is the same, while each weekend day in a month is the same too. The calculation interval is one hour.

(3) Each decision variable is initialized with random values (within physical ranges). The inertia weight coefficient is updated in each iteration as follows.

$$\omega = \omega_{max} - (\omega_{max} - \omega_{min})/N_{iter}k \tag{38}$$

(4) When the iterations are converged, $L_{hot}(k)$, $L_{cld}(k)$, $DNI_{start}(k)$, $t_{sunset}(k)$, $DNI_{insalt}(k)$ and $W(k)$ are the optimization results on the k th day.

(5) Repeat (2)-(4) until $k = n$.

(6) The total power generation W_{final} is the sum of the power generated on each day, which is calculated using daily optimal values of L_{hot}, L_{cld}, DNI_{start}, t_{sunset} and DNI_{insalt}.

$$W_{final} = \sum_{k=1}^{n} W(k) \tag{39}$$

The rolling optimization model based on holism with $l = 2$ is shown in Fig. 9 [35,36], and the scheme of the R-PSO algorithm is shown in Fig. 10.

4.3. Optimization constraints

(1) Constraints of the receiver model

It is assumed that the maximum mass flow rate at the inlet and outlet of the receiver is the same. The parameters of the receiver are constrained as:

$$Q_{sum}(t) = Q_{rx,o}(t) + Q_{sto}(t) \tag{40}$$

$$Q_{rx,o}(t) \geqslant 0 \tag{41}$$

$$\dot{Q}_{field}(t) \geqslant \dot{Q}_{hf}(t) \geqslant \dot{Q}_{rx,min} \tag{42}$$

$$DNI_{start} \geqslant DNI_{start,min} \tag{43}$$

$$t_{sunset} \geqslant t_{rx,min} \tag{44}$$

$$DNI_{insalt} \geqslant DNI_{insalt,min} \tag{45}$$

$$T_{s,des,max} \geqslant T_{rx,o}(t) \geqslant 0 \tag{46}$$

$$\dot{m}_{rx,des} \geqslant \dot{m}_{rx,i}(t) \geqslant 0 \tag{47}$$

$$\dot{m}_{rx,des} \geqslant \dot{m}_{rx,o}(t) \geqslant 0 \tag{48}$$

Equations (40)-(42) bound the energy at the inlet and outlet of the receiver where t is time. Q_{sum} [J] is the total thermal energy that is provided by the TES and receiver at Minute t. $Q_{rx,o}$ [J] is the thermal energy production from the receiver. $\dot{Q}_{field}$ [W] is the maximum thermal power that the heliostat field can reflect onto the receiver. $\dot{Q}_{rx,min}$ [W] is the minimum thermal power for the operation of heliostat field.

Equations (43)-(45) bound the DNI for the receiver to start operating DNI_{start}, the minimum minutes before sunset for the receiver to start operating t_{sunset}, and the DNI for the receiver to start feeding salt DNI_{insalt}. $DNI_{start,min}$, $t_{rx,min}$ and $DNI_{insalt,min}$ are the minimum value of the above parameters.

Equations (46)-(48) bound the salt temperature at the outlet $T_{rx,o}$ and the salt mass flow rate at the inlet $\dot{m}_{rx,i}$ and outlet $\dot{m}_{rx,o}$ of the receiver. $T_{s,des,max}$ is the maximum design salt temperature. $\dot{m}_{rx,des}$ is the maximum design mass flow at the inlet and outlet of the receiver.

(2) Constraints of the TES model

The parameters of the TES are constrained as:

$$\dot{m}_{sto,cld,i}(t) + \dot{m}_{sto,hot,i}(t) + \dot{m}_{rx,i}(t) = \dot{m}_{sto,cld,o}(t) + \dot{m}_{sto,hot,ot}(t) + \dot{m}_{rx,o}(t) \tag{49}$$

$$Q_{sto}(t) \geqslant Q_{sto,min} \tag{50}$$

$$L_{cld}(t) \geqslant L_{cld,min} \tag{51}$$

$$L_{hot}(t) \geqslant L_{hot,min} \tag{52}$$

$$L_{hot}(t) > L_{hot,min,o} \tag{53}$$

$$L_{cld}(t) \geqslant L_{cld,min,o} \tag{54}$$

$$T_{s,des,max} \geqslant T_{sto,hot}(t) \tag{55}$$

$$T_{sto,cld}(t) \geqslant T_{s,des,min} \tag{56}$$

Equation (49) constrains the mass flow at the inlet and outlet of cold and hot tanks, where $\dot{m}_{sto,cld,i}$, $\dot{m}_{sto,hot,i}$, $\dot{m}_{sto,cld,o}$ and $\dot{m}_{sto,hot,o}$ are the salt mass flow rate at the inlet and outlet of cold and hot tanks, respectively. $m_{rx,i}$ and $m_{rx,o}$ are the mass flow at the inlet of the receiver in the feeding salt stage and the outlet of the receiver in the draining salt stage. Equation (50) constrains the thermal energy stored in the TES, where $Q_{sto,min}$ is the minimum thermal energy stored in the hot tank when the steam turbine is operating. L_{cld} and L_{hot} are the liquid levels in cold and hot tanks. $L_{cld,min}$ and $L_{hot,min}$ are the minimum liquid levels in cold and hot tanks. The minimum liquid levels of cold and hot tanks are constrained by Equations (51) and (52) instead of directly limiting the thermal energy stored in the TES. Equation (53) limits the liquid level in hot tank for the steam turbine to start reducing load and shutdown. Equation (54) constrains the liquid level in cold tank for the receiver to start draining salt. $L_{cld,min,o}$ and $L_{hot,min,o}$ are the minimum operating liquid levels in cold and hot tanks. Equations (55) and (56) limit the salt temperature in hot and cold tanks. $T_{s,des,min}$ is the minimum design salt temperature in the STP plant.

(3) Constraints of the heat exchanger model

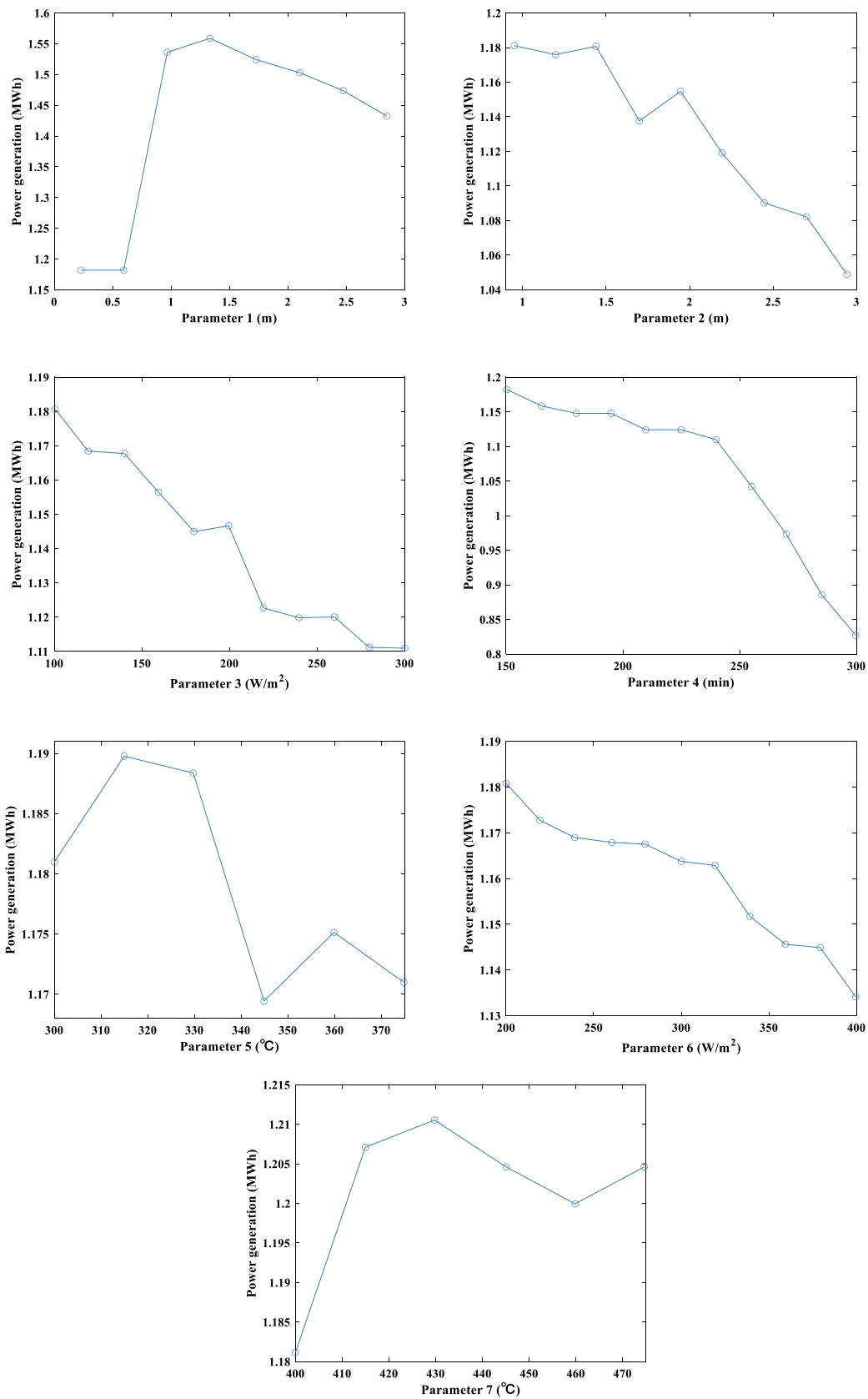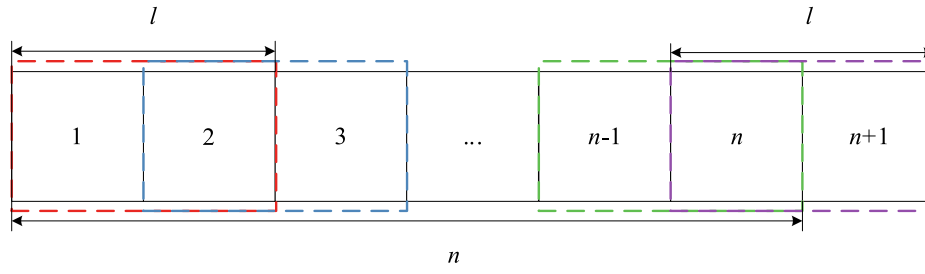**Fig. 8.** Power generation with respect to the 7 parameters.

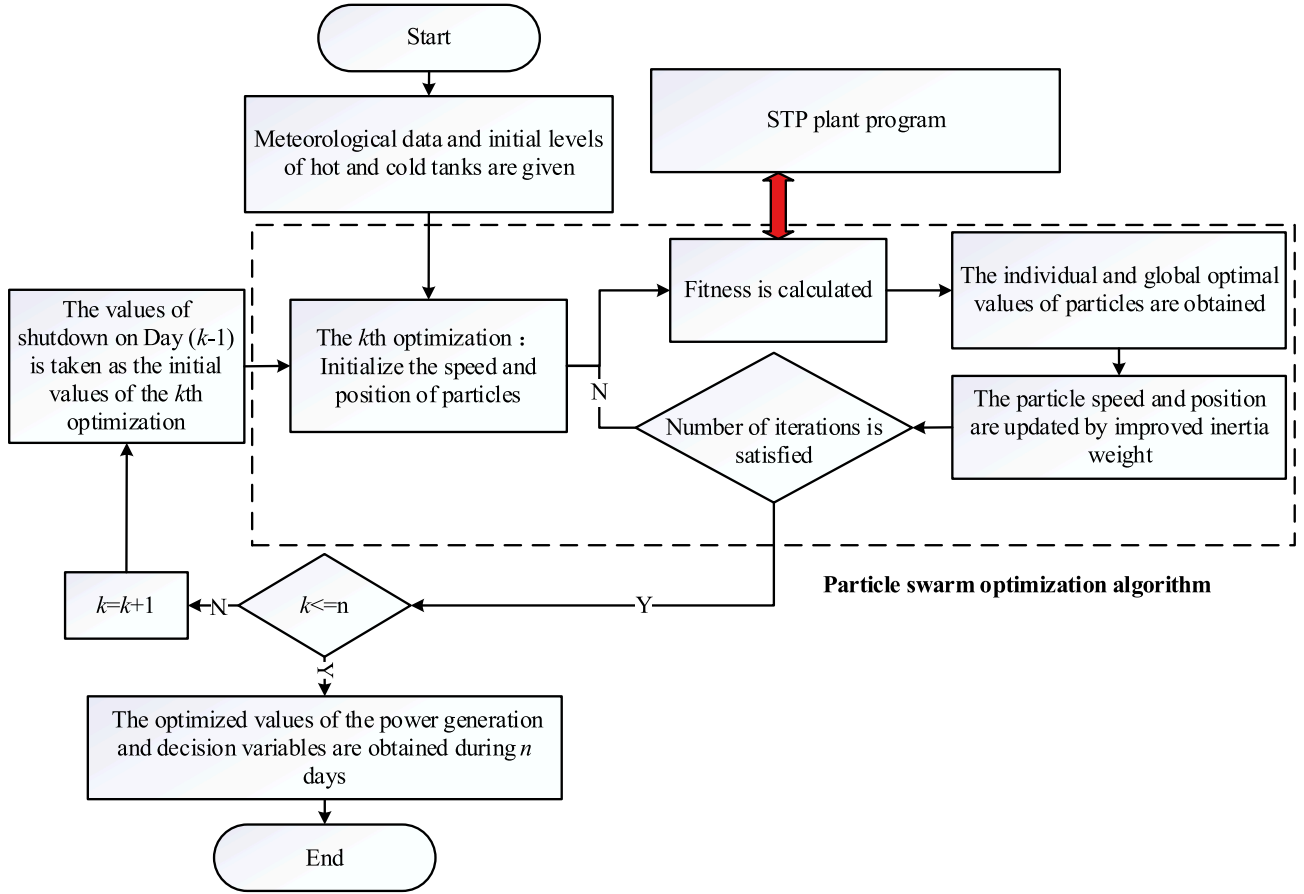**Fig. 9.** The rolling optimization model based on holism.

Fig. 10. The scheme of the R-PSO algorithm.

The parameters of the heat exchanger are constrained as:

$$\dot{m}_{\text{blr,sob}}(t) \geqslant 0 \tag{57}$$

$$T_{\text{s,des,min}} \leqslant T_{\text{pre,s,o}}(t) \leqslant T_{\text{s,des,max}} \tag{58}$$

$$T_{\text{sto,c}}(t) \leqslant T_{\text{sup,s,i}}(t) \leqslant T_{\text{sto,h}}(\text{t}) \tag{59}$$

$$T_{\text{sto,c}}(t) \leqslant T_{\text{r,s,i}}(t) \leqslant T_{\text{sto,h}}(\text{t}) \tag{60}$$

$$\dot{m}_{\text{ex,s,max}} \geqslant \dot{m}_{\text{ex,s}}(t) \geqslant 0 \tag{61}$$

$$\dot{m}_{\text{ex,w,max}} \geqslant \dot{m}_{\text{ex,w}}(t) \geqslant 0 \tag{62}$$

Equation (57) is the salt extraction constraint. Equation (58) limits the salt temperature at the outlet of the preheater. Equations (59) and (60) constrain the salt temperature at the inlets of the superheater and reheater, where $T_{\text{sup,s,i}}$ and $T_{\text{r,s,i}}$ are the salt temperatures at the inlets of the superheater and reheater, respectively. Equations (61) and (62)

constrain the mass flows of molten salt and water in the heat exchanger ($\dot{m}_{\text{ex,s}}$ and $\dot{m}_{\text{ex,w}}$), where $\dot{m}_{\text{ex,s,max}}$ and $\dot{m}_{\text{ex,w,max}}$ are the maximum mass flows of molten salt and water in the heat exchanger, respectively.

(4) Constraints of the steam turbine model

The parameters of the steam turbine are constrained as [2,37,38]:

$$Q_{\text{sum}}(t) \geqslant Q_{\text{s,steam}} \tag{63}$$

$$P_{\text{min}} \leqslant P(t) \leqslant P_{\text{rate}} \tag{64}$$

$$t_{\text{lower,state}} \leqslant t_{\text{stop}} < t_{\text{upper,state}} \tag{65}$$

$$T_{\text{lower,steam}} \leqslant T_{\text{m,steam}} < T_{\text{upper,steam}} \tag{66}$$

$$-R^{\text{down}} \leqslant P(t) - P(t-1) \leqslant R^{\text{up}} \tag{67}$$

$$t_{\text{st,on}} \geqslant t_{\text{st,on,min}} \tag{68}$$

$$t_{\text{st,off}} \geqslant t_{\text{st,off,min}} \tag{69}$$

Equation (63) constrains the operation condition of the steam turbine, where $Q_{s,steam}$ is the minimum thermal energy provided by TES and receiver for the steam turbine to start operating. Equation (64) constrains the power of the steam turbine P, where P_{min} and P_{rate} are the minimum power and the rated power of the steam turbine, respectively. Equation (65) is used to check the start-up state of the steam turbine. t_{stop} is the shutdown duration at the last time. $t_{lower,state}$ and $t_{upper,state}$ indicate the lower and upper limits of the shutdown duration in the stage of the cold, warm, hot, or extreme hot start-up. Equation (66) is used to check the operation stage in the start-up state of the steam turbine, where $T_{m,steam}$ is the steam temperature in the high-pressure cylinder, $T_{lower,steam}$ and $T_{upper,steam}$ represent the lower and upper limits of the temperature in the operation stage of steam turbine, including the main steam temperature and pressure rise, reheated steam temperature and pressure rise, turning or grid-connection of the steam turbine. Equation (67) limits the climbing capacity of the steam turbine, where R^{up} and R^{down} are the maximum up and down climbing capacities of the steam turbine, respectively. Equations (68) and (69) limit the minimum operation duration and shutdown duration of the steam turbine ($t_{st,on}$ and $t_{st,off}$), and $t_{st,on,min}$ and $t_{st,off,min}$ are the minimum operation duration and the minimum shutdown duration. Other constraints for the operation state of the steam turbine in the STP plant are similar to the steam turbines from a fossil-fuel power plant.

5. Results and discussion

In this section, the optimization results of operational thresholds of a 50 MW STP plant in Northwest China are presented. The maximum and minimum design temperatures of molten salt are 565℃ and 290℃, respectively [23]. The minimum operating liquid levels in storage tanks are taken as 8 % of the tank height. The maximum climbing rate of the steam turbine in the STP plant is 10 %/min. Due to the information-sharing agreement with the STP plant, other constraint values cannot be listed here. One-minute averaged DNI data (Fig. 11) for the corresponding periods are used for the optimization. The power generation of the first 14 days in each quarter over one year is optimized by PSO and R-PSO, and the results are compared with the ones without optimization. The R-PSO algorithm is used for optimizing operation strategy,

with the length of each optimization stage is taken as 2 days. It takes about 1.3 h to optimize the two days using a computer with 8 GB RAM and Intel Core i5-104000 CPU @ 2.90 GHz. The computation time is sufficient to meet the needs of day-ahead scheduling.

The daily optimized values of Parameters 1, 2, 3, 4, and 6 are shown in Fig. 12. Compared with the PSO values, the R-PSO values of the five parameters in each quarter are not the same for each day. Most of the R-PSO values are lower than the PSO values, with a few occasions exceed the PSO values. The variation of Parameters 1, 2, and 6 is inversely proportional to the variation of the DNI value as shown in Fig. 11. The maximum and minimum values are obtained in Quarters 2 and 3, respectively. The value in Quarter 1 is higher than that in Quarter 4. It is concluded that the higher the DNI value, the less liquid needs to be reserved in the tanks. Parameters 3 and 4 are the largest in Quarter 1, and the smallest in Quarter 2, indicating that the receiver is relatively affected when the DNI value is small.

The daily power generation of the STP plant calculated by PES with pre-defined operational thresholds without optimization, PES with PSO, and PES with R-PSO are shown in Fig. 13. From Fig. 13, it can be seen that certain compromise of local interests would result in global maximum interests. For example, as shown in Fig. 13 c), although the unoptimized results on Day 5 and Day 6 are slightly higher than the optimized results, the optimized result on Day 8 is much higher than the unoptimized result, resulting to improved total power generation from Days 5 to 8. This phenomenon can also be reflected in Fig. 13 d), although the optimized result is 115 MWh less than the unoptimized result on Day 8 to Day 11, it is 165 MWh more than the unoptimized one on Day 12 to Day 14, resulting in 50 MWh increased total power generation from Days 8 to 14. Therefore, the optimization goal is to maximize the annual power generation.

The total power generation of each quarter is presented in Table 3. The total power generation for the studying period calculated by the three models is 25265, 27454, and 28,651 MWh, respectively. Compared with the power generation PES without optimization, the power generation calculated with PSO increases by 8.66 %, and the power generation calculated with R-PSO increases by 13.4 %. Therefore, the optimization of Parameters 1, 2, 3, 4, and 6 can substantially improve the operation strategy and increase the power generation of STP plant.
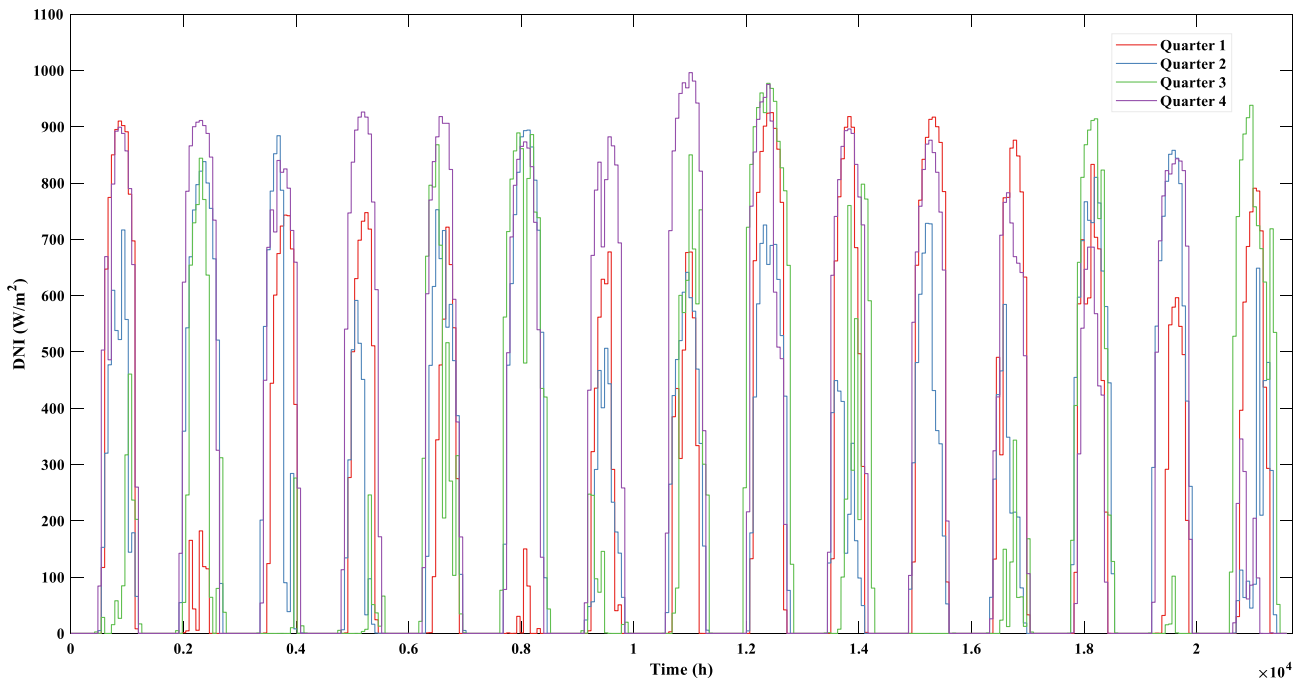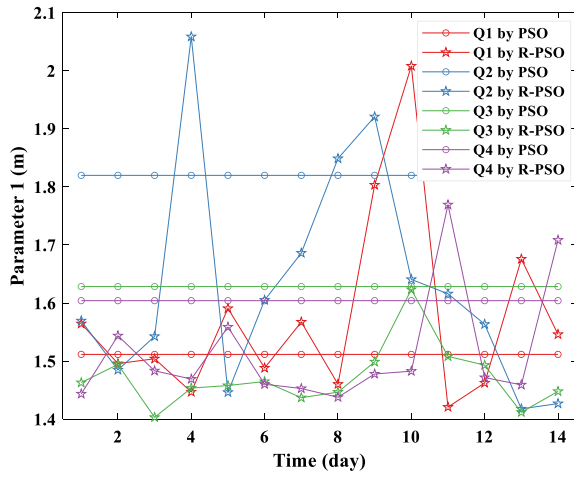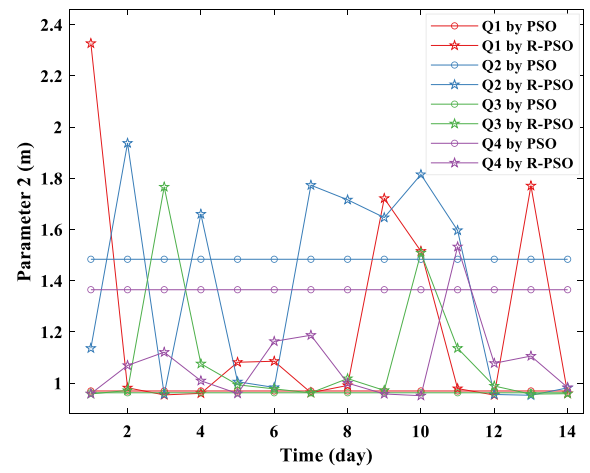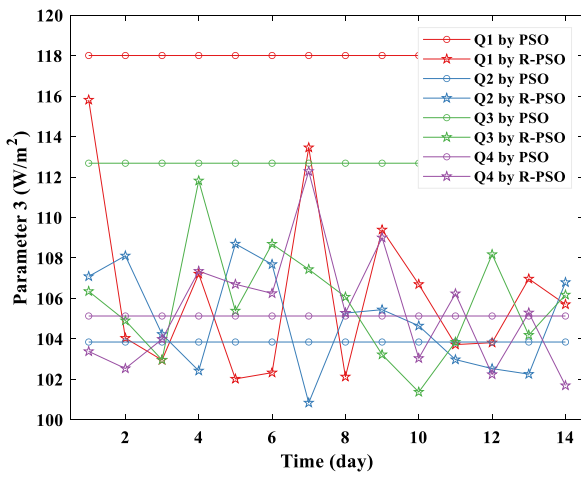

Fig. 11. The 1-min averaged DNI value for the first 14 days of each quarter.
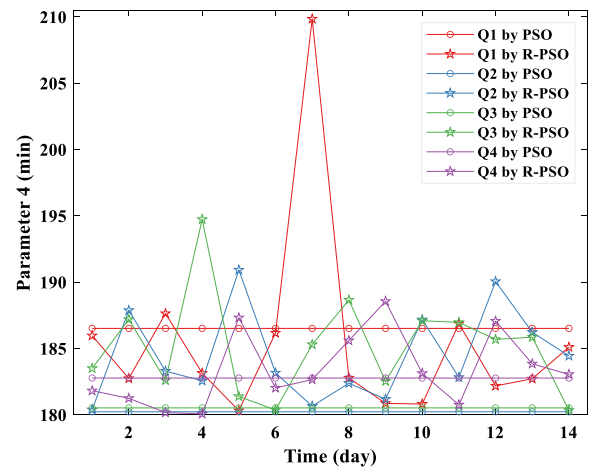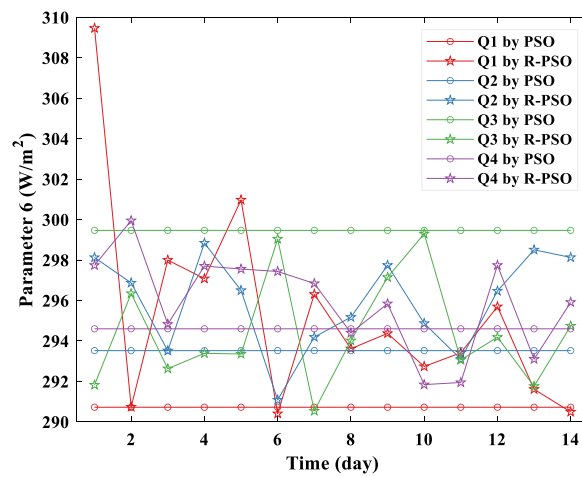
Fig. 12. Daily optimized values of Parameters 1, 2, 3, 4 and 6 during the first 14 days of each quarter. (a) Parameter 1; (b) Parameter 2; (c) Parameter 3; (d) Parameter 4 and (e) Parameter 6.
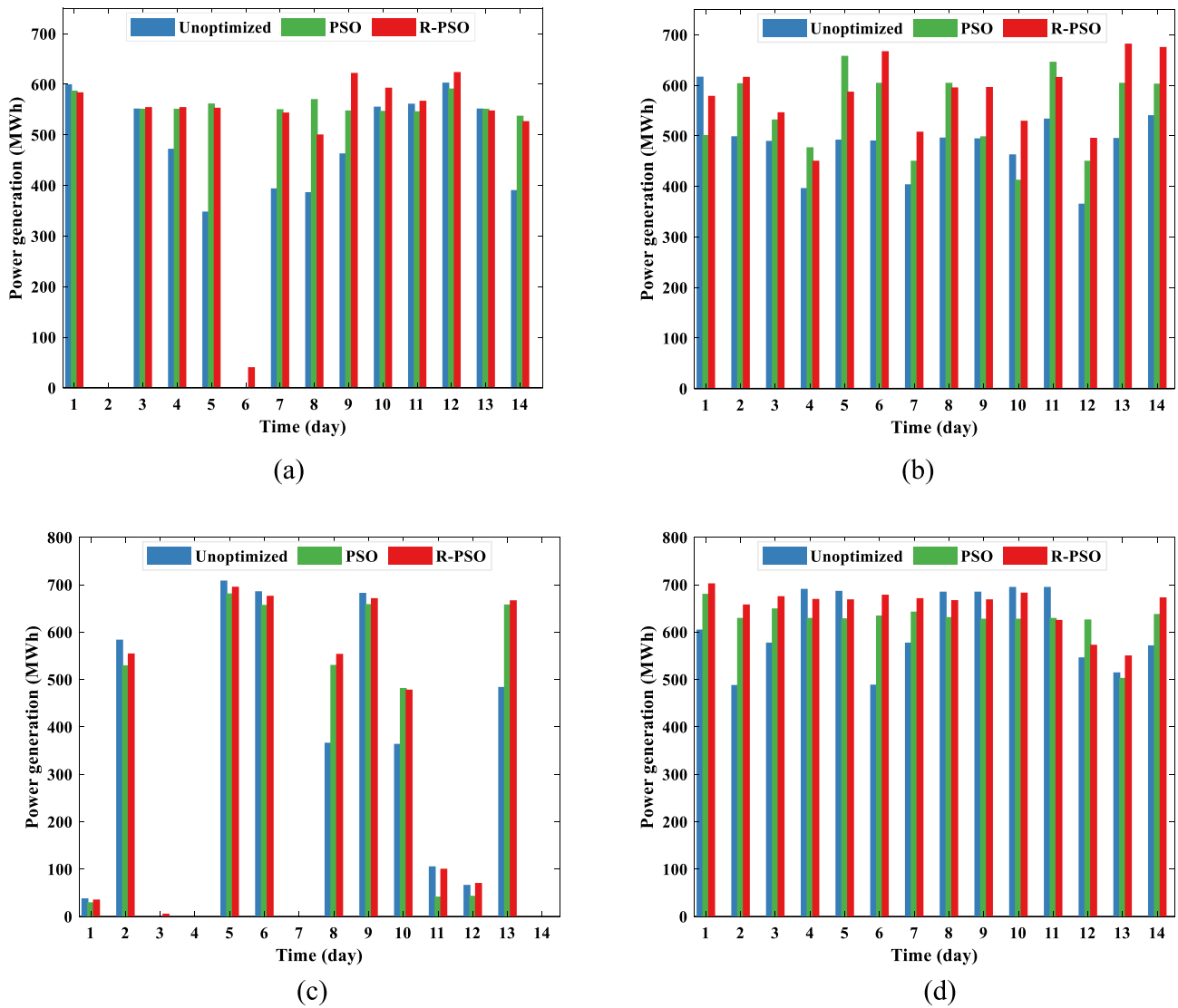
Fig. 13. Daily power production of the STP plant for (a) the first 14 days of Quarter 1; (b) the first 14 days of Quarter 2; (c) the first 14 days of Quarter 3 and (d) the first 14 days of Quarter 4.

Moreover, as shown in Table 3, 41 % of the output with R-PSO is greater than 50 % of the rated power in STP, which is 18 % higher than that in the unoptimized case. Meanwhile, 43 % of the output from R-PSO is between 25 % and 50 % of the rated power, which is 16 % lower than that in the unoptimized case. Therefore, R-PSO effectively reduces the proportion of steam turbine generator units in low-load operation.

The hourly power generation in the first 14 days of Quarter 1 is shown in Fig. 14, and the daily start-up time of the steam turbine is shown in Fig. 15 (value zero on the ordinate indicates that the steam turbine is not started on the day). The sharp changes of the curve are due to high temporal resolution (one minute) of the calculation. It can be seen from the figure that the calculation with R-PSO is not to maximize the power generation of the STP plant during the day. Instead, the operational thresholds of the day are preset according to future solar radiation data, and to control the start-up time of the steam turbine for the next day, so as to maximize the total power generation of the STP plant within the calculation period.

The hourly liquid levels of the hot tank and cold tank in the first 14 days of Quarter 1 are shown in Fig. 16 and Fig. 17, respectively. It can be seen that the daily lowest liquid level calculated by PES with R-PSO in the hot tank is higher, while the daily highest liquid level in the cold tank is lower, because a certain amount of hot salt is left in the hot tank to

control the start-up time of the receiver and steam turbine in the next stage.

6. Conclusions

To increase the annual power generation of solar tower power plants (STP) with thermal energy storage, a software with detailed models and an operational strategy based on rolling optimization with holism is proposed in this paper. The conclusions are as follows:

(1) A minute-wise in-house numerical model of solar tower power plants, capsulate as the PES software, is proposed. The close-to-engineering module models and easy-to-tune operation strategy under all conditions are included. The annual total power generation calculated by PES and System Advisor Model (SAM) is 177,062 MWh and 179,890 MWh, respectively, which has only 1.57 % difference. The average difference in monthly power generation between the two software is less than 3.9 %. The comparisons of hourly power generation also show similar results. When compared with SAM, and PES have more detailed parameters and more flexible modules that can better fulfill our purpose of operational threshold optimization.

(2) The effects of operational thresholds on the power generation of STP plants are analyzed by PES. Five thresholds that have strong

Table 3

Total power generation for the first 14 days of each quarter.

Items	PES without Optimization	PES with PSO	PES with R- PSO
Total power generation for the first 14 days of Quarter 1, MWh	5881	6699	6818
Total power generation for the first 14 days of Quarter 2, MWh	6783	7654	8150
Total power generation for the first 14 days of Quarter 3, MWh	4088	4316	4513
Total power generation for the first 14 days of Quarter 4, MWh	8513	8785	9170
Summation, MWh	25,265	27,454	28,651
Average daily power generation, MWh	451.16	490.25	511.63
Maximum daily power generation, MWh	708.76	681.68	702.93
Standard deviation of daily power generation, MWh	210.26	217.52	220.44
Occurrence percentage of the power between 20 % and 50 % of its rated power, %	59	40	43
Occurrence percentage of the power greater than 50 % of its rated power, %	23	40	41

correlations with power generation are identified: (a) the liquid level in hot tank for the steam turbine to start reducing load and shutdown, (b) the liquid level in cold tank for the receiver to start draining salt, (c) the DNI for the receiver to start operating, (d) the minutes before sunset for the receiver to be able to start operating and (e) the DNI for the receiver to start feeding salt.

(3) The operation strategy is developed by rolling optimization based on holism improved particle swarm optimization (R-PSO). It distinguishes the model operation stage and state through the operation characteristics of each model and future irradiation resources, and optimizes the daily threshold values of the models. The average daily power generation calculated by PES without optimization, with PSO, and with R-PSO are 451.16 MWh, 490.25 MWh, and 511.63 MWh, respectively. The total power generation calculated by PES with R-PSO is 13.40 % higher than that without optimization, and 4.36 % higher

than that with only PSO. Therefore, the total power generation can be improved significantly by the proposed R-PSO algorithm.

In the future, other advanced optimization algorithms based on rolling optimization and holism could be explored, so as to further improve the overall power generation of solar tower power plants.

CRediT authorship contribution statement

Chen Wang: Conceptualization, Methodology, Investigation, Writing – original draft. **Su Guo:** Resources, Supervision, Funding acquisition. **Huanjin Pei:** Software. **Yi He:** Data curation, Formal analysis. **Deyou Liu:** Validation, Supervision. **Mengying Li:** Validation.

Declaration of Competing Interest

The authors declare that they have no known competing financial interests or personal relationships that could have appeared to influence
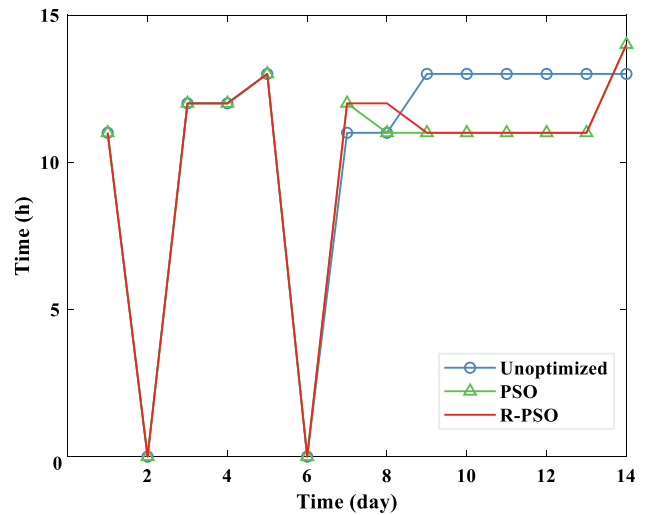

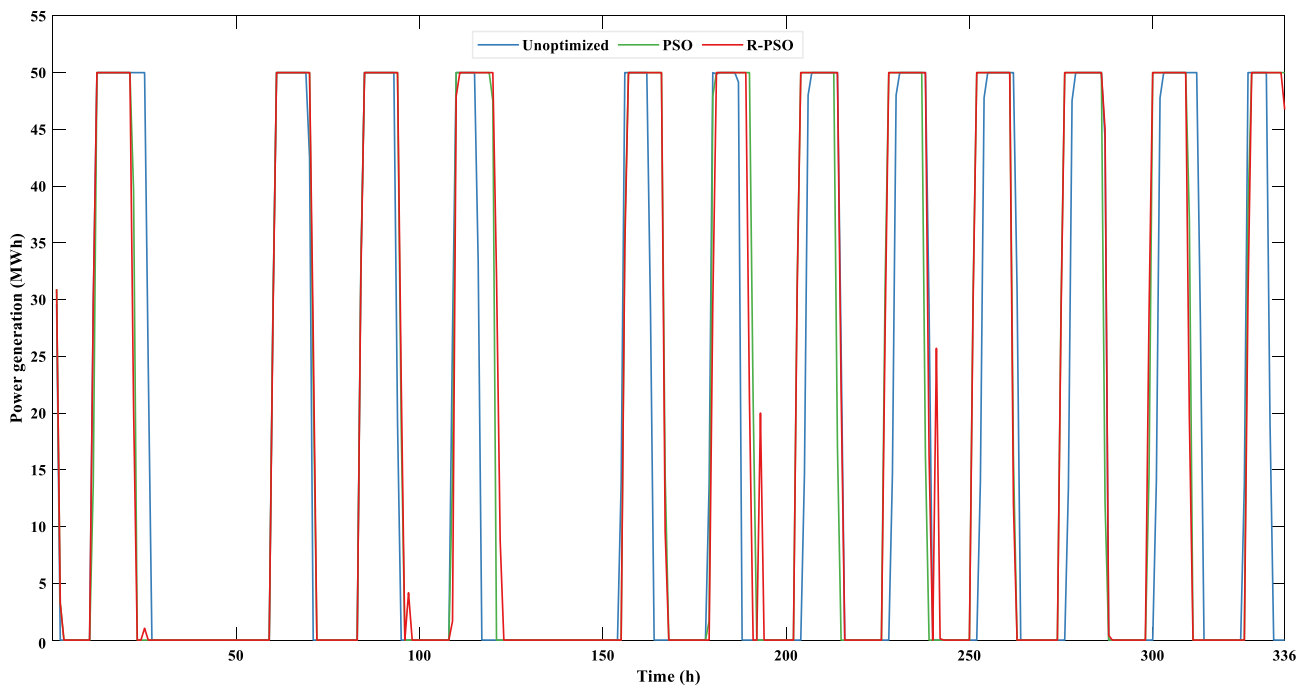**Fig. 15.** Start-up time of the steam turbine.

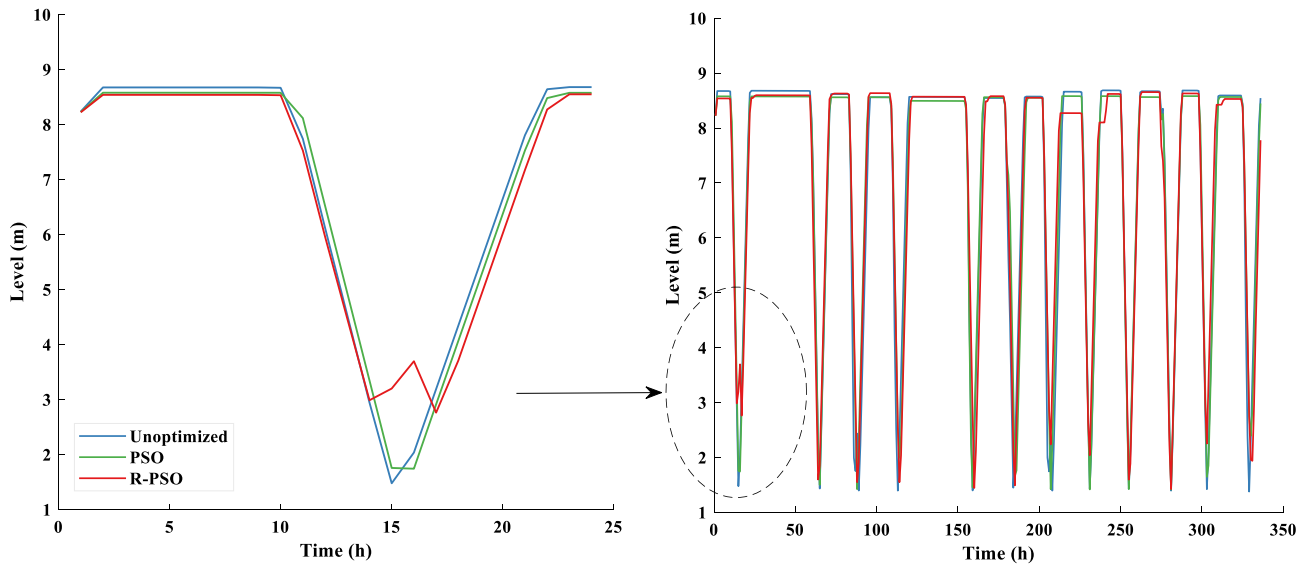**Fig. 14.** Hourly power generation of the STP plant for the first 14 days of Quarter 1.

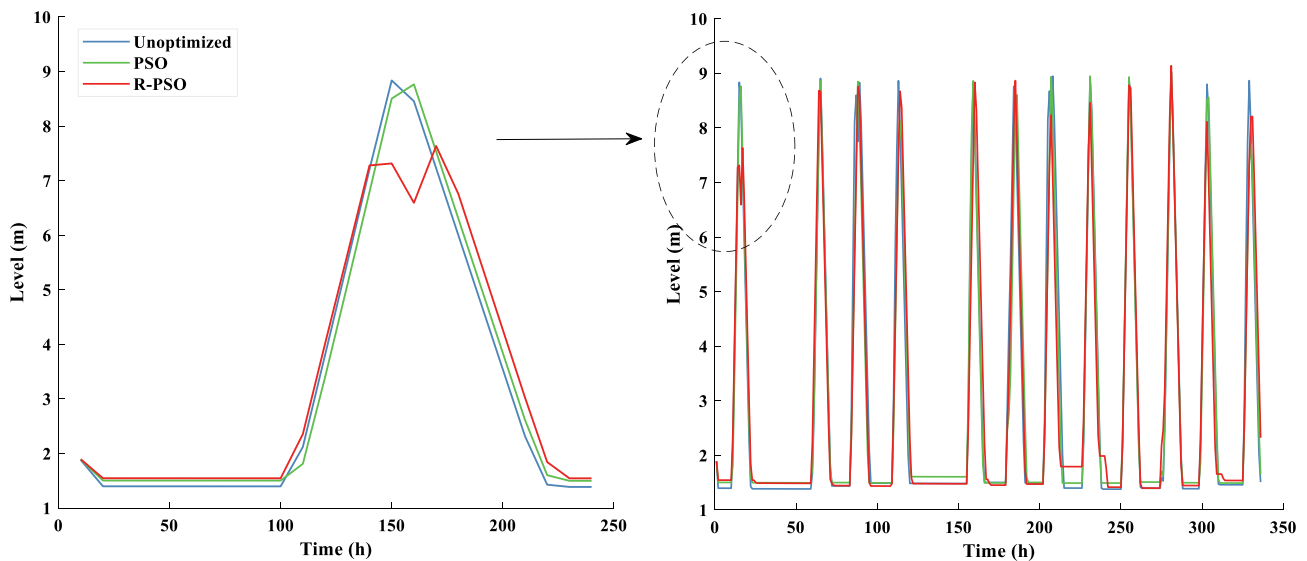**Fig. 16.** The liquid level of the hot salt tank.

Fig. 17. The liquid level of the cold salt tank.

the work reported in this paper.

Data availability

The data that has been used is confidential.

Acknowledgements

References

[1] Kebede AA, Kalogiannis T, Van Mierlo J, Berecibar M. A comprehensive review of stationary energy storage devices for large scale renewable energy sources grid integration. Renew Sustain Energy Rev 2022;159:112213.

[2] Yang Y, Guo S, Liu D, Li R, Chu Y. Operation optimization strategy for wind-concentrated solar power hybrid power generation system. Energy Convers Manag 2018;160:243–50.

[3] Ellingwood K, Mohammadi K, Powell K. Dynamic optimization and economic evaluation of flexible heat integration in a hybrid concentrated solar power plant. Appl Energy 2020;276:115513.

[4] Kiefer CP, del Río P. Analysing the barriers and drivers to concentrating solar power in the European Union. Policy implications J Clean Prod 2020;251:119400.

[5] Ling-zhi R, Xin-gang Z, Yu-zhuo Z, Yan-bin L. The economic performance of concentrated solar power industry in China. J Clean Prod 2018;205:799–813.

[6] Besarati SM, Goswami DY. A computationally efficient method for the design of the heliostat field for solar power tower plant. Renew Energy 2014;69:226–32.

[7] Piroozmand P, Boroushaki M. A computational method for optimal design of the multi-tower heliostat field considering heliostats interactions. Energy 2016;106: 240–52.

[8] Rodríguez-Sánchez MR, Soria-Verdugo A, Almendros-Ibáñez JA, Acosta-Iborra A, Santana D. Thermal design guidelines of solar power towers. Appl Therm Eng 2014;63:428–38.

[9] Luo Y, Du X, Wen D. Novel design of central dual-receiver for solar power tower. Appl Therm Eng 2015;91:1071–81.

[10] Wang J, Guo L, Zhang C, Song L, Duan J, Duan L. Thermal power forecasting of solar power tower system by combining mechanism modeling and deep learning method. Energy 2020;208:118403.

[11] Benammar S, Khellaf A, Mohammedi K. Contribution to the modeling and simulation of solar power tower plants using energy analysis. Energy Convers Manag 2014;78:923–30.

[12] Xu C, Wang Z, Li X, Sun F. Energy and exergy analysis of solar power tower plants. Appl Therm Eng 2011;31:3904–13.

[13] Dobos A, Neises T, Wagner M. Advances in CSP simulation technology in the system advisor model. Energy Procedia 2014;49:2482–9.

[14] Saghafifar M, Gadalla M, Mohammadi K. Thermo-economic analysis and optimization of heliostat fields using AINEH code: Analysis of implementation of non-equal heliostats (AINEH). Renew Energy 2019;135:920–35.

[15] Marugán-Cruz C, Serrano D, Gómez-Hernández J, Sánchez-Delgado S. Solar multiple optimization of a DSG linear Fresnel power plant. Energy Convers Manag 2019;184:571–80.

[16] Lee K, Lee I. Optimization of a heliostat field site in central receiver systems based on analysis of site slope effect. Sol Energy 2019;193:175–83.

[17] Atif M, Al-Sulaiman FA. Optimization of heliostat field layout in solar central receiver systems on annual basis using differential evolution algorithm. Energy Convers Manag 2015;95:1–9.

[18] Khosravi A, Malekan M, Pabon J, Zhao X, Assad MEH. Design parameter modelling of solar power tower system using adaptive neuro-fuzzy inference system optimized with a combination of genetic algorithm and teaching learning-based optimization algorithm. J Clean Prod 2020;244:118904.

[19] Alirahmi SM, Dabbagh SR, Ahmadi P, Wongwises S. Multi-objective design optimization of a multi-generation energy system based on geothermal and solar energy. Energy Convers Manag 2020;205:112426.

[20] Zhang W, Maleki A, Rosen MA, Liu J. Optimization with a simulated annealing algorithm of a hybrid system for renewable energy including battery and hydrogen storage. Energy 2018;163:191–207.

[21] Mayer MJ, Szilágyi A, Gróf G. Environmental and economic multi-objective optimization of a household level hybrid renewable energy system by genetic algorithm. Appl Energy 2020;269:115058.

[22] Wu F, Chen Z, Lin X. GB-T 40614–2021 Technical requirement of performance evaluation for solar thermal power plant. Stand Press China; 2021.

[23] Wagner MJ. Simulation and predictive performance modeling of utility-scale central receiver system power plants 2008.

[24] Deng L, Wu Y, Guo S, Zhang L, Sun H. Rose pattern for heliostat field optimization with a dynamic speciation-based mutation differential evolution. Int J Energy Res 2020;44:1951–70.

[25] Su G, Deyou L. The calculating of the shadow and block efficiency of the heliostats considering tower shadows in tower SPPs. Acta Energiae Solaris Sin 2007;28:1182.

[26] Su G. Design of heliostat field, CPC and roof CPV of solar tower power plant. Master Thesis. Hohai University, 2006.

[27] Guo Su, Jin Yihao, Wang Jiale, Ji Wenjia. A calculation method of the energy flux density distribution of the solar receiver. Patent, ZL201910909833.2 2021.

[28] Biggs F, Vittitoe CN. The HELIOS model for the optical behavior of reflecting solar concentrators. Sandia National Lab.(SNL-NM), Albuquerque, NM (United States); 1979.

[29] Sassi G. Some notes on shadow and blockage effects. Sol Energy 1983;31:331–3.

[30] Guo T. Research on key control technologies of solar thermal power plants with tower. Doctoral Thesis. Hohai University, 2011.

[31] Wagner MJ, Gilman P. Technical manual for the SAM physical trough model. National Renewable Energy Lab.(NREL), Golden, CO (United States); 2011.

[32] Hagen BA, Nikolaisen M, Andresen T. A novel methodology for Rankine cycle analysis with generic heat exchanger models. Appl Therm Eng 2020;165:114566.

[33] Zhang Q, Wang Z, Du X, Yu G, Wu H. Dynamic simulation of steam generation system in solar tower power plant. Renew Energy 2019;135:866–76.

[34] Mei S, Wang Y, Liu F. A game theory based planning model and analysis for hybrid power system with wind generators-photovoltaic panels-storage batteries. Dianli Xitong ZidonghuaAutomation Electr Power Syst 2011;35:13–9.

[35] Silvente J, Kopanos GM, Pistikopoulos EN, Espuña A. A rolling horizon optimization framework for the simultaneous energy supply and demand planning in microgrids. Appl Energy 2015;155:485–501.

[36] Cao Z, Han Y, Wang J, Zhao Q. Two-stage energy generation schedule market rolling optimisation of highly wind power penetrated microgrids. Int J Electr Power Energy Syst 2019;112:12–27.

[37] Chen R, Sun H, Guo Q, Li Z, Deng T, Wu W, et al. Reducing generation uncertainty by integrating CSP with wind power: an adaptive robust optimization-based analysis. IEEE Trans Sustain Energy 2015;6:583–94.

[38] Guo S, He Y, Pei H, Wu S. The multi-objective capacity optimization of wind-photovoltaic-thermal energy storage hybrid power system with electric heater. Sol Energy 2020;195:138–49.